Local Dynamics and Stability of Apocytochrome b_{562} Examined by Hydrogen Exchange†

Ernesto J. Fuentes and A. Joshua Wand*

Departments of Chemistry and Biological Sciences and Center for Structural Biology, State University of New York at Buffalo, Buffalo, New York 14260-3000

Received October 17, 1997; Revised Manuscript Received December 19, 1997

ABSTRACT: Cytochrome b_{562} is a heme-binding protein consisting of four helices folded into a classic helix bundle motif. Though retaining much of the topology of the holoprotein, apocytochrome b_{562} displays physical features commonly associated with so-called protein molten globules. Here, the stability and dynamics of this "structured" molten globule are probed by examination of the dependence of its hydrogen exchange behavior upon the presence of a chemical denaturant. Compared to other systems studied in this manner, apocytochrome b_{562} displays a limited dynamic range of hydrogen exchange rates and the analysis required the development of a quantitative approach. The protein is found to have three regions of subglobal cooperative stability. The most stable region, or core, is composed of the central two helices of the bundle, with the N- and C-terminal helices being of independent and lower stability. The dependence of the global unfolding free energy upon denaturant concentration indicates the applicability of a binding model and explains the observed difference between global unfolding free energies obtained by the linear extrapolation method and those obtained by calorimetry and hydrogen exchange. These observations place a significant restraint upon the type of folding pathway that is operative for this protein and suggest that that the N- and C-terminal helices fold and unfold independently of the core of the molecule.

Cytochrome b_{562} is a classic example of a four-helix bundle protein. It consists of 106 amino acid residues (12 kD) which form four separate helices, two of which contain the axial ligands that bind a prosthetic b-type heme moiety. The crystal structure of the holoprotein (*1*, *2*) and the solution structure of the apostate of the protein (*3*) have been determined. Although these structures share the same gross topology, some important distinctions are noteworthy. Three of the four helices in the holoprotein are well represented in the solution structure of the apoprotein ((*3*) see Figure 1) while the C-terminal helix (helix IV) of the former is somewhat ill-defined in the latter (*3*). The two middle helices of the apoprotein superimpose very well with their counterparts in the holoprotein. Most of the variance between the structures of the holo and apo states of the protein arises from the relative packing of helix I and IV against the two middle helices. Rather than repack its core, the apoprotein maintains a large cavern that is highly exposed to solvent (*3*). This structural feature explains many of the peculiar physical properties of the protein (*3*) such as its relatively low ΔC_p for unfolding (*4*) and its relatively low stability to chemical and thermal denaturation (*4*).

The structural consequences of the removal of a prosthetic group have been examined in other proteins such as cytochrome *c* (*5*), myoglobin (*6*−*9*), and cytochrome b_5 (*10*). These proteins display a large range of destabilization and structural reorganization. Generally, they feature extensive native secondary and tertiary structure and comprise a class of metastable proteins that display some but not all the attributes of a classic "molten globule".

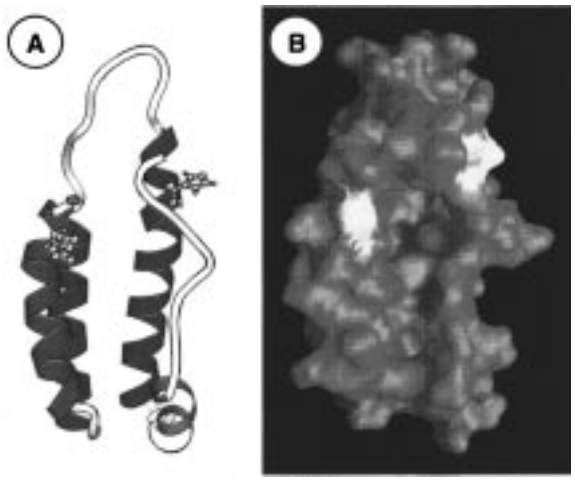

FIGURE 1: Structure of apocytochrome b_{562} determined by NMR spectroscopy. Shown in panel A is a ribbons representation (*52*) of the refined average structure (PDB code 1APC) determined by Feng et al. (*3*). The protein is oriented with helix I on the left and helix IV on the right. Shown in panel B is a molecular surface representation (*53*) of the protein in the same orientation. Note the large cavern that is readily accessible to solvent. Highlighted in yellow are Met-7 (left) and His-102 (right) which provide axial ligands to the heme in the holoprotein.

Insight into the free energy relationships underlying fundamental units of protein structure can be gained by a variety of approaches. A particularly appealing method has recently been introduced and relies upon the promotion of hydrogen exchange (HX)[1] by chemical denaturants such as guanidinium hydrochloride (GdmCl) (*11*−*13*). Using cy-

† Supported by Grant GM 35940 from the National Institutes of Health and Grants DAAH04-96-1-0312 and DAAG55-97-10181 from the Army Research Office awarded to A.J.W.

* To whom correspondence should be addressed.

S0006-2960(97)02579-8 CCC: $15.00
Published on Web 02/24/1998

tochrome *c* as an example, Englander and co-workers have interpreted the promotion of hydrogen exchange by chemical denaturants by considering the contribution of local, subglobal, and global motions leading from the native (hydrogen-bonded and hydrogen exchange incompetent state) to hydrogen exchange competent states (*13*, *14*). In a view based on the promotion of various hydrogen exchange competent states by the binding of denaturants to newly accessible surface area, local, subglobal, and global hydrogen exchange mechanisms are distinguished by their differential sensitivity to denaturant via the treatments of Tanford, Pace, and others (*15*−*18*).

In the case of cytochrome *c*, the dependence on chemical denaturant of the effective free energy changes leading from the native to various hydrogen exchange competent states allowed the definition of a putative kinetic folding pathway. This remarkable result of obtaining significant insight into kinetic folding processes from measurements made essentially at equilibrium has led us to apply this approach to apocytochrome b_{562}. Here, we seek to define the fundamental units of cooperative structure within the unusual protein state occupied by apocytochrome b_{562}.

MATERIALS AND METHODS

Expression and Purification of Cytochrome b_{562}. Cytochrome b_{562} was obtained using a previously described expression system (*19*) or one utilizing a T7-based promoter. The latter construct was prepared using the polymerase chain reaction to span the cytochrome b_{562} gene from the 5′ signal sequence to the 3′ *Sal*I restriction site (*19*). A *Bam*HI restriction site was incorporated into the sense primer to facilitate subsequent cloning reactions. The purified cytochrome b_{562} gene fragment was ligated to a modified pET-15b plasmid (Novagen) containing a *Bam*HI and *Sal*I site and subsequently transformed into *Escherichia coli* cells, strain BL21(DE3). The cytochrome b_{562} sequence was verified by dideoxy DNA sequencing. Yields in minimal media were increased nearly 5-fold over plasmid pNS2207, typically yielding nearly 40 mg of purified protein/L of culture media. The availability of such an expression system permitted the use of ^{1}H-^{15}N correlated spectroscopy for the determination of amide hydrogen exchange rates. Expression of cytochrome b_{562} from either plasmid was carried out in the appropriate cell line in minimal media containing M9 salts using $^{15}NH_4Cl$ (1 g/L) (Isotec) as sole nitrogen source. δ-Aminolevulinic acid, a heme precursor (Sigma), was added (20 mg/L) to enhance the expression of holocytochrome b_{562}. Protein purification was carried out essentially as described previously (*4*, *19*, *20*) with only slight modification: acid precipitation and chromatography were carried out at pH 4.35−4.55 and gel filtration chromatography was determined to be unnecessary and was not performed. The protein product was analyzed by electrospray mass spectroscopy (Washington University, St. Louis) and SDS−PAGE electrophoresis. Obtained apocytochrome b_{562} was judged to be >95% pure. The protein concentration was determined using optical spectroscopy and a molar extinction coefficient of 3 mM^{-1} cm^{-1} (*4*).

NMR Spectroscopy. NMR samples (650 μL) contained ∼2−3 mM apocytochrome b_{562} in a buffer comprised of 10 mM sodium d_3-acetate (Isotec) and 0.65 M of KCl and/or GdmCl as required at pH* 4.5. Samples were prepared by hydrating 20−25 mg of lyophilized protein with 65 μL of the buffer prepared with H_2O. The hydrated sample was centrifuged to remove insoluble particulate matter. The hydrogen exchange reaction was initiated by dilution of the sample with 585 μL of the buffer prepared with D_2O. The dead-time of the experiment, defined as the time from the addition of D_2O buffer to initiation of the NMR experiment, was on the order of 20−25 min. The pH of the sample was determined after the completion of the HX experiment using a conventional micro glass electrode. Solutions of GdmCl were prepared from a stock solution whose concentration was determined by refractometry (*21*). Hydrogen exchange rates were determined using serial two-dimensional sensitivity-enhanced gradient-selected ^{1}H-^{15}N HSQC spectra (*22*) using Varian Unity-INOVA spectrometers operating at 500 and 600 MHz for ^{1}H. The spectra were collected as 64 complex points in the incremented ^{15}N evolution time domain (t_1) and 1024 complex points in the acquisition time domain (t_2). The length of each experiment was approximately 15 or 30 min (8 or 16 scans per free induction decay, respectively). Sequential ^{1}H-^{15}N HSQC spectra were collected up to 3000 min, as required. The data were baseline corrected, and the H_2O solvent peak was digitally removed. Each dimension was zero filled and subjected to a $\pi/2$ sine squared apodization function. Each resulting two-dimensional data matrix consisted of 1024 × 512 points. The data were processed using Felix (Biosym Technologies Inc.). A three-dimensional NOESY−HSQC (*23*) data set was recorded to resolve any assignment issues for the data collected at pH 4.5 and 25 °C as opposed to the conditions corresponding to the original resonance assignments (*24*).

Analysis of Hydrogen Exchange Rates. Denaturant concentrations used in this study (up to 0.60 M GdmCl) caused only minor perturbation of the ^{1}H-^{15}N HSQC cross-peak positions. The intensities of each cross-peak at each time point for each HX experiment were plotted against time in minutes and fitted to a general three parameter single-exponential equation using a nonlinear least-squares Levenberg−Marquardt method (*25*). Uncertainty in the raw data was provided by the RMS difference in signal intensity in regions of the 2D spectrum containing no cross-peaks. Random coil hydrogen exchange rates, k_{chem}, were calculated for each exchangeable backbone amide hydrogen, taking into account nearest neighbor and inductive effects (*26*) and solution conditions (isotope content, pH, temperature) (*27*). The ionization state of acidic side chains (Glu and Asp) were estimated by using the pK_a of the free amino acid. The equilibrium constant for the opening reaction, K_{op}, was calculated using eq 2. Slowing factors (SF) are the inverse of K_{op}. Effective free energies for opening leading to hydrogen exchange, ΔG_{HX}^{eff}, were calculated using eq 3.

Accessible surface areas of folded states were calculated using the Connolly algorithm as implemented in the molec-

[1] Abbreviations: GdmCl, guanidinium hydrochloride; NMR, nuclear magnetic resonance; HX, hydrogen exchange; pH*, observed pH meter reading uncorrected for the isotope effect; CD, circular dichroism; DSC, differential scanning calorimetry; HSQC, heteronuclear single-quantum correlation; NOESY, nuclear Overhauser effect spectroscopy; LEM, linear extrapolation method; ΔG_{LEM}, free energy for global unfolding obtained from linear extrapolation method; ΔG_{cal}, free energy for global unfolding obtained from differential scanning calorimetry; ΔG_{HX}, free energy for global unfolding obtained from hydrogen exchange; SF, hydrogen exchange slowing factor.

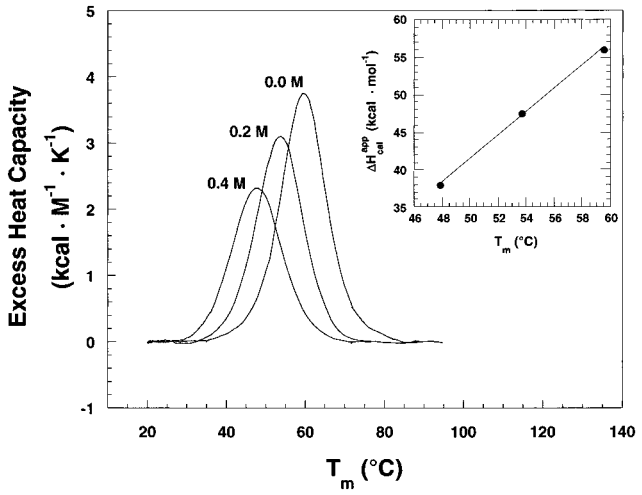

FIGURE 2: Calorimetric estimates of the heat of unfolding of apocytochrome b_{562} in the absence and presence of GdmCl. Samples were appoximately 3.7 mg/mL in protein and were prepared in 10 mM sodium acetate buffer in 90% D_2O, 0.65 M NaCl, and pH* 4.5. The Inset shows a plot of the ΔH_{cal}^{app} versus T_m obtained at the various GdmCl concentrations employed, these are uncorrected for the effects of denaturant desolvation (see text).

ular analysis program Insight II (Biosym Technologies). The accessible surface area of the unfolded molecule and partialy unfolded forms was approximated using the method of Creamer et al. (*28*, *29*). The change in accessible surface area, ΔASA, was defined as the increase in surface area due to unfolding using the native, fully folded structure as reference.

Determination of Global Stability. Differential scanning calorimetry (DSC) was carried out in a Calorimetry Sciences NanoDSC. Analysis employed the vendor supplied software. Protein samples were generally ∼3.7 mg/mL and were exhaustively dialyzed and centrifuged before use. Solvent conditions were the same as those for HX experiments, 90% D_2O in the presence of 10 mM sodium acetate at pH* 4.5, and either 0, 0.2, or 0.4 M GdmCl. Solvent baselines were scanned repeatedly. Protein DSC data were obtained at a rate of 60 °C/h and repeated twice on each sample. Calorimetrically obtained enthalpies, ΔH_{cal}^{app}, are uncorrected for the contribution of desolvation of denaturant (see below).

Circular dichroism measurements were carried out in a Jasco J500C spectropolarimeter at 222 nm at 25 °C. Solvent conditions were the same as those for HX and DSC experiments, 90% D_2O in the presence of 10 mM sodium acetate at pH* 4.5 and the required amount of GdmCl. The unfolding equilibrium constant at each GdmCl concentration was determined by subtracting the pre- and post-transition baselines from the primary data (*18*). The standard linear extrapolation method (LEM) was used to determine the free energy of unfolding, ΔG_{LEM}.

RESULTS

Thermal and Chemical Denaturation of Apocytochrome b_{562}. Over the pH range used throughout this work (pH* 4.5−5.2), apocytochrome b_{562} displays a fully reversible, moderately cooperative, and apparently two-state thermal unfolding profile (Figure 2 and unpublished results). Differential scanning calorimetry was carried out under solution conditions identical with those used for the hydrogen exchange studies described below, i.e., in addition to identical buffer and salts, the isotopic content of the solvent was 90% deuterium. The integrated form of the Gibbs−Helmholtz equation relates the free energy for unfolding to the ΔC_p and ΔH_{cal}.

$$\Delta G = \Delta H\left(\frac{T_m - T}{T_m}\right) + (T - T_m)\Delta C_p - T\Delta C_p \ln\left(\frac{T}{T_m}\right) \quad (1)$$

Direct determination of ΔC_p of unfolding by differential scanning calorimetry is somewhat problematic. Estimates of ΔC_p for the unfolding of apocytochrome b_{562} range between 0.36 and 1.0 kcal mol^{-1} K^{-1} (*3*, *4*; Robinson et al., personal communication). The holoprotein exhibits a larger ΔC_p range of 1.0−2.4 kcal mol^{-1} K^{-1} depending on solution conditions (*3*, *4*; Robinson et al., personal communication). Consequently, an upper limit of 1.0 kcal mol^{-1} K^{-1} is placed on ΔC_p of the apoprotein. An independent estimate of ΔC_p is also available from the dependence of the heats of unfolding at various denaturant concentrations (*30*−*32*). A plot of the apparent ΔH_{cal} obtained at 0, 0.2, and 0.4 M GdmCl is linear (inset to Figure 2) and has a slope of about 1.5 kcal mol^{-1} K^{-1}. This apparent ΔC_p contains a contribution from the desolvation of the denaturant which, for GdmCl, has been estimated to be on the order of 1 kcal mol^{-1} K^{-1} (*30*, *31*). This suggests that ΔC_p for the unfolding of apocytochrome b_{562} is on the order of 0.5 kcal mol^{-1} K^{-1}, which is in good agreement with values determined by others (Robinson et al., personal communication). Using this value as a consensus of the calorimetric data available for this protein and the ΔH_{cal} obtained here gives a ΔG_{cal} for unfolding of approximately 5 kcal mol^{-1} in the absence of denaturant. ΔG_{cal} is sensitive to the presence of GdmCl in a nonlinear way (see refs *31* and *32* and Figure 3). It should also be pointed out that the van't Hoff enthalpies obtained from fits of the calorimetry data ranged to within 10−15% of ΔH_{cal}.

When followed by changes in the CD spectrum, the denaturation of the protein with GdmCl is found to be moderately cooperative and apparently two-state with a midpoint denaturation concentration of ∼1.1 M. The dependence on GdmCl is apparently linear over this concentration range having associated free energy change and slope of 3.3 kcal mol^{-1} and 5.8 kcal mol^{-1} M^{-1}, respectively (Figure 3).

Native State Hydrogen Exchange. Using serial ^{1}H-^{15}N HSQC NMR spectroscopy, hydrogen exchange rates for 60 of 102 amide protons in apocytochrome b_{562} could be measured at pH* 4.5 and 25 °C in the presence of 0.65 M KCl. Hydrogen exchange rates greater than ∼3 h^{-1} could not be determined using this method. Examples of hydrogen exchange curves obtained for the amide of Ala-37 are shown in Figure 5 and serve to illustrate the quality of data obtained over the range of hydrogen exchange rates that can be quantified. The precision of obtained rate constants estimated from analysis of residuals to the fits averaged 0.89% relative error over all data obtained. Replicates of hydrogen exchange data sets gave an average variance in the obtained apparent free energy of 0.21 kcal mol^{-1} (see eq 3 below).

Assuming that the rate of closing (k_{cl}) from the hydrogen exchange competent state(s) to the hydrogen-bonded, ex-

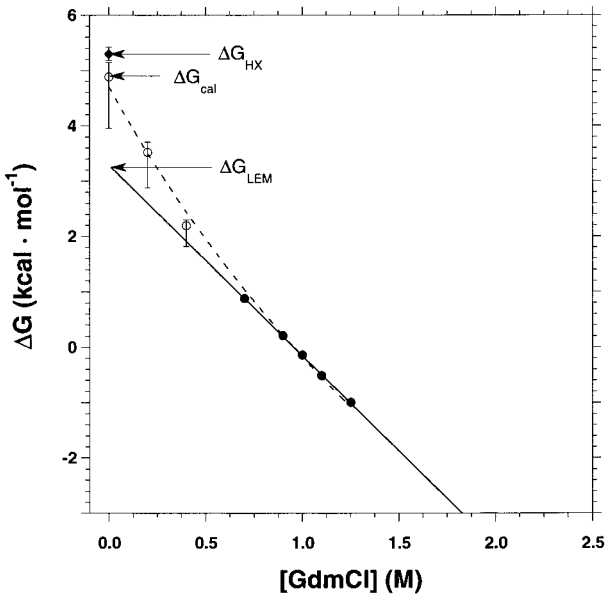

FIGURE 3: Apparent free energy of unfolding of apocytochrome b_{562} obtained from linear extrapolation of GdmCl denaturation monitored by far-UV circular dichroism and by differential scanning calorimetry. Denaturation data obtained at GdmCl concentrations of 0.7−1.25 M (closed circles, solid line), corresponding to 18 and 84% unfolded, were used extrapolate to zero denaturant. Samples were 4 μM in protein and were prepared in 10 mM sodium acetate buffer in 90% D_2O, 0.65 M NaCl, pH* 4.5 and 25 °C. Calorimetric estimates of the free energy of unfolding (open circles), obtained using the same buffer as used for the hydrogen exchange and CD measurements, were calculated using ΔH_{cal}^{app} measured at 0, 0.2, and 0.4 M GdmCl and a ΔC_p of 0.5 kcal mol^{-1} K^{-1}. Error bars represent the range in free energy calculated using the integrated form of the Gibbs−Helmholtz equation and employing ΔC_p values of 0.36 and 1.0 kcal mol^{-1} K^{-1} (*4*; Robinson et al., personal communication). Regression of the obtained ΔG_{cal} and ΔG_{LEM} to the Tanford denaturant binding model (eq 8) (dashed line) yielded $K_b = 0.69$ and $\Delta n = 15.8$. Estimates of the global unfolding free energy in the absence of denaturant measured by hydrogen exchange (corrected for the proline effect), calorimetry and LEM are also indicated.

change incompetent state is much faster than the rate of chemical catalysis, the so-called EX2 condition prevails, and the effective equilibrium opening constant (K_{op}) can be obtained from the observed rate of exchange (k_{obs}) and knowledge of the underlying chemical rate (k_{chem}) using eq 2 (*33*, *34*).

$$k_{obs} = \frac{k_{op}}{k_{op} + k_{cl}} k_{chem} \approx \frac{k_{op}}{k_{cl}} k_{chem} = K_{op} k_{chem} \qquad (2)$$

Here we have used the usual assumption that $k_{cl} \gg k_{op}$ allowing the indicated simplification. The definition of k_{chem} is now routinely available by use of empirical calibrations for sequence specific effects and the effects of solution and thermal conditions upon the chemistry of hydrogen exchange (*26*, *27*).

Slowing factors (SF) determined for apocytochrome b_{562} are plotted as a function of residue number in Figure 6. The range of determined slowing factors spans approximately 2 orders of magnitude reaching a maximum of 10^4 and a minimum of approximately 10^2. It is clear that four distinct regions of protection exist, each encompassing a region known to be helical in the solution structure of the apoprotein (*3*). There is a good correspondence with hydrogen-bonding

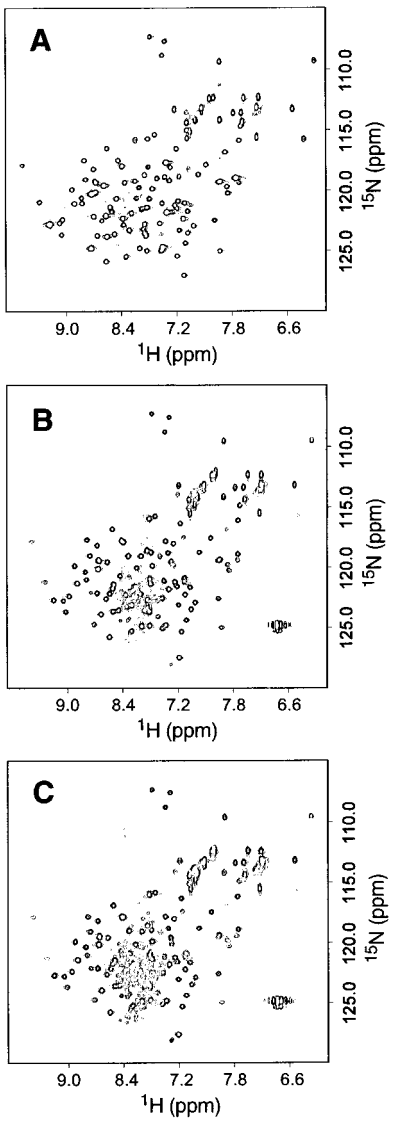

FIGURE 4: Sensitivity of the ^{15}N-HSQC spectrum of apocytochrome b_{562} to the presence of GdmCl. Shown are ^{15}N-HSQC spectra collected at 750 MHz (^{1}H) obtained under similar solution conditions as the hydrogen exchange data: 90% D_2O/10% H_2O 10 mM sodium acetate buffer, pH* 4.5, 25 °C and (A) no GdmCl, 0.65 M NaCl, (B) 0.65 M GdmCl, 0.0 M NaCl, (C) 0.70 GdmCl, 0.0 M NaCl.

seen in the apocytochrome b_{562} solution structure. Particularly interesting is the absence of significantly slowed (i.e., greater than 10^2) amide hydrogens in the last 10 residues of the protein. This region is helical in the holoprotein structure, shows helical-like NMR spectral parameters in the apoprotein (*24*) but is ill-defined in the corresponding structural model (*3*). This could in principle be due to inadequate structural restraints and/or the presence of extensive dynamics (*3*, *35*). The absence of significantly slowed hydrogen exchange in this region of the protein indicates that if helical, it is only marginally stable.

If the slowest amide hydrogens are moved to a hydrogen exchange competent state(s) only upon global unfolding of the protein, then the stability of the protein can be estimated from the slowing factors obtained for these sites by use of eq 3 (*33*, *34*).

$$\Delta G_{HX}^{eff} = -RT \ln K_{op} \qquad (3)$$

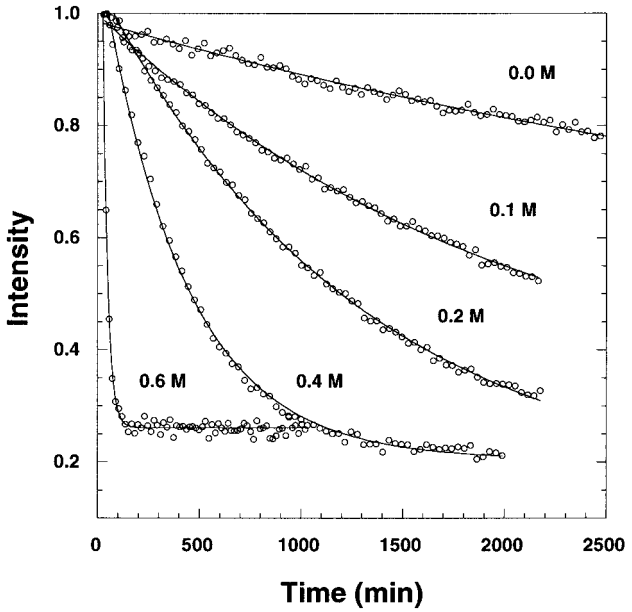

FIGURE 5: Representative amide hydrogen exchange curves. Normalized intensities of Ala-37 ^{15}N-^{1}H correlation cross-peaks in serially acquired ^{15}N-HSQC spectra for various concentrations of GdmCl. The effective dead-time for the experiment is approximately 20 min and the obtained rates span 0.011−2.5 h^{-1}.

This approach would suggest that the amides of residues 32−37 exchange with a global unfolding event associated with a free energy change of approximately 5.9 kcal mol^{-1}. This is somewhat higher than the estimates provided by the differential scanning calorimetry and linear extrapolation from chemical denaturation as followed by circular dichroism summarized above. We will return to this later.

Hydrogen Exchange in the Presence of Chemical Denaturant. The effect of GdmCl on the NMR spectrum of apocytochrome b_{562} is quite minor at concentrations of denaturant at or below 0.60 M. However, at GdmCl concentration above 0.60 M, the ^{1}H-^{15}N spectrum begins to collapse presumably due to chemical exchange effects arising from significant interconversion of the folded and unfolded states of the protein (Figure 4). Accordingly, all hydrogen exchange data presented here was obtained at GdmCl concentrations less than or equal to 0.60 M. Hydrogen exchange rates for apocytochrome b_{562} were obtained at GdmCl concentrations ranging from 0 to 0.60 M under constant ionic strength. A total of 15 experiments were conducted at 10 concentrations of GdmCl ranging between 0 and 0.60 M. Replicate measurements at 0 M (×2), 0.1 M (×2), 0.4 M (×2), 0.5 M (×3), and 0.6 M (×2) GdmCl allowed for an estimation of the precision of the obtained rates. As expected from eq 4, the general effect of GdmCl is to accelerate hydrogen exchange (see Figures 4 and 5). The analysis of this primary data rests significantly upon the assumption that exchange is indeed in the EX2 limit. The EX2 limit provides access to the free energy of opening via eq 3, which is only valid when $k_{cl} \gg k_{chem}$. It has been pointed out (*36*) that the binding of denaturant to the open state can significantly slow the return of the protein to the folded state such that the EX2 condition is lost. Thus, although the basic chemistry of hydrogen exchange virtually guarantees the EX2 limit under conditions used here (pH* 4.5, 25 °C) in the absence of denaturant, the dominance of the EX2 limit in the presence of denaturant requires confirmation. A direct test of the EX2 condition is to vary the pH at which exchange is carried out and confirm that the change in observed hydrogen exchange rate is as predicted by the corresponding change in k_{chem} (*13*). Such a test was carried out under the highest GdmCl concentration employed (0.60 M). Logarithms of hydrogen exchange rates obtained at pH* 4.71 and 5.17 showed a linear correlation (slope ∼0.8) with correlation coefficient of 0.9, thus reinforcing the expectation that the EX2 condition is present.

Analysis of Mechanisms of Hydrogen Exchange. There are now several examples of the use of chemical denaturants to promote hydrogen exchange in proteins (*11*, *36*−*38*). Englander and co-workers have provided a framework within which to relate the dependence of hydrogen exchange rates on chemical denaturants to the character of the physical motion(s) of the protein underlying the hydrogen exchange event (i.e., K_{op} of eq 2, for a review, see ref *14*). Simply stated, they propose that the acceleration of hydrogen exchange by chemical denaturants such as GdmCl is related to the stabilization of the exchange competent state relative to the native (exchange incompetent state) by the increase in surface area available for the binding of the denaturant to the protein. The relationship between the free energy change associated with hydrogen exchange (see eq 3) and denaturant concentration is often assumed to be linear and is then given by Pace (*18*):

$$\Delta G^{\mathrm{eff}}_{\mathrm{HX}}(\mathrm{GdmCl}) = \Delta G^{\mathrm{eff}}_{\mathrm{HX}}(0) - mRT[\mathrm{GdmCl}] \quad (4)$$

The critical observation is that different types of physical motion(s) leading to hydrogen exchange competent states may lead to states that result in different associated changes in accessible surface area. Hence, they will be distinguishable on the basis of their effective "*m*" values and that amides participating in a common motion will then have a common *m* value. Furthermore, one can imagine that motions involving smaller regions of the protein will expose smaller surface areas and will therefore have smaller *m* values. Similarly, global unfolding of the protein is anticipated to produce the largest possible increase in accessible surface area and is therefore expected to have the largest *m* value associated with it. Bai et al. (*14*) have developed this notion to propose that hydrogen exchange can occur via local, subglobal, or global mechanisms leading to exchange competent state(s). In the limit of small $K^{\mathrm{eff}}_{\mathrm{HX}}$, we have

$$K^{\mathrm{eff}}_{\mathrm{HX}} = K^{\mathrm{local}}_{\mathrm{HX}} + K^{\mathrm{subglobal}}_{\mathrm{HX}} + K^{\mathrm{global}}_{\mathrm{HX}} \quad (5)$$

Recasting eq 5 in terms of eq 4 gives a general relationship for the dependence of hydrogen exchange of a given amide hydrogen on the concentration of chemical denaturant, [Den].

$$K^{\mathrm{eff}}_{\mathrm{HX}} = K^{\mathrm{local}}_{\mathrm{HX}}\exp(m_{\mathrm{l}}[\mathrm{Den}]/RT) + K^{\mathrm{subglobal}}_{\mathrm{HX}}\exp(m_{\mathrm{sg}}[\mathrm{Den}]/RT) + K^{\mathrm{global}}_{\mathrm{op}}\exp(m_{\mathrm{g}}[\mathrm{Den}]/RT) \quad (6)$$

Furthermore, the so-called local motions appear to have little or no increase in accessible surface area associated with them and have *m* values approaching zero. The task is to not only to obtain the various *K* and *m* parameters for each amide hydrogen but also to identify which sites participate in cooperative motions involving sets of amides. Obviously, those amides which exchange, in whole or in part, through

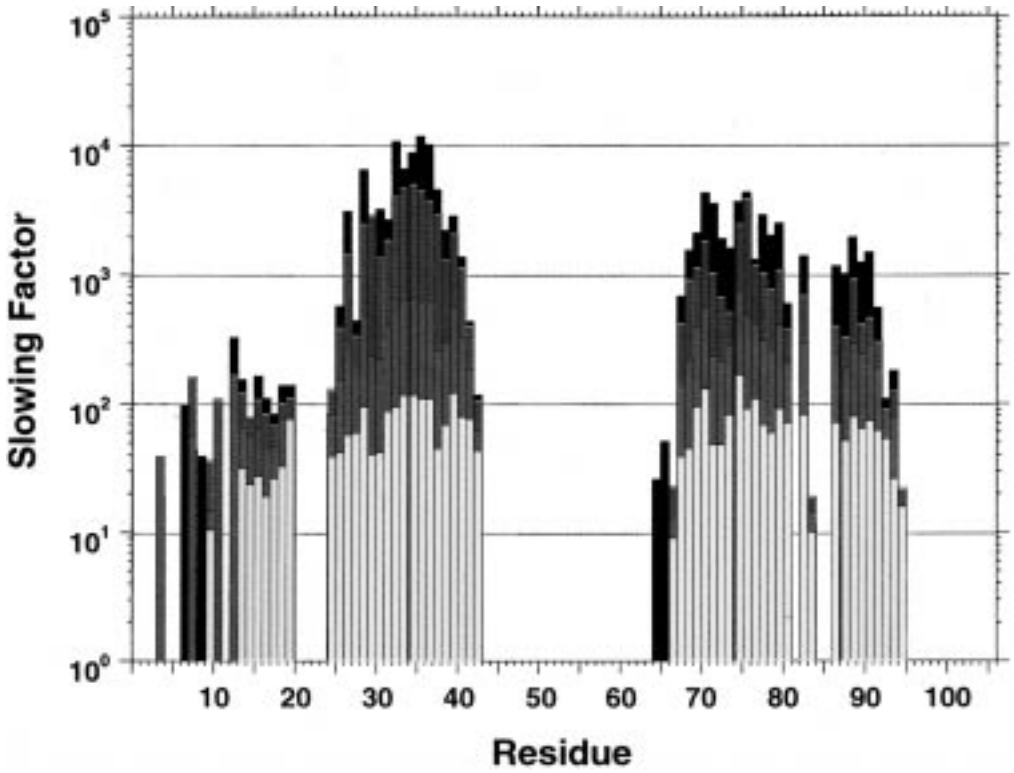

FIGURE 6: Hydrogen exchange profiles for apocytochrome b_{562} as a function of GdmCl. The slowing factors versus sequence position obtained at four of the eight GdmCl concentrations examined are shown (0.0, black; 0.2, green; 0.4, red; 0.6 M, yellow). Primary hydrogen exchange data was obtained at pH* 4.63−4.87 in 10 mM sodium phosphate buffer with the indicated GdmCl and sufficient NaCl to maintain a salt concentration of 0.65 M. Slowing factors were calculated using the known solution conditions and the empirical parameters of Bai et al. (*26*).

a common exchange competent state will have common *m* and *K* parameters contributing to K_{HX}^{eff}.

In this view, subglobal openings will have greater *m* values than those of local openings but smaller than the *m* value dictated by the global opening. Thus, as the concentration of denaturant increases, the global term, having the largest *m* value, will ultimately dominate K_{HX}^{eff}. At low concentrations of denaturant, the term having the largest contribution to the equilibrium opening constant will dominant. Under these conditions, the dominant contribution may often be due to local fluctuation term which can be distinguished by its small effective *m* value. Equations 5 and 6 also point out that when a single mechanism dominates, a linear relationship between ΔG_{HX}^{eff} and denaturant concentration exists. This overall behavior suggests a hierarchical approach to the analysis of the dependence of hydrogen exchange upon denaturant concentration.

To provide a quantitative footing for the evaluation of a postulated collection of amide hydrogens as participating in the same subglobal opening, we introduce an error function describing the degree of correspondence between the observed ΔG_{HX}^{eff}s obtained and those predicted on the basis of proposed set of *K* and *m* parameters, i.e.,

$$\text{Error} = \sum_{i,j}^{N,M}\left(\frac{\Delta G_{HX,obs}^{eff}(NH_i,[Den]_j) - \Delta G_{HX,calc}^{eff}(NH_i,[Den]_j)}{\Delta G_{HX,obs}^{eff}(NH_i,[Den]_j)}\right)^2 \quad (7)$$

Here, *N* is the number of amide hydrogens in the proposed set and *M* is the number of denaturant concentrations at which data is available. $\Delta G_{HX,obs}^{eff}$ and $\Delta G_{HX,calc}^{eff}$ are the observed and calculated ΔG_{HX}^{eff} at a given amide site and denaturant concentration, the latter given by eq 6 and the current set of *K* and *m* parameters. The *K* and *m* parameters that are required are sampled over a grid of all reasonable values and the error function tabulated. This approach was introduced for the analysis of NMR relaxation and has been used successfully to analyze equations having similar numerical properties (*39*). To assess the reliability of obtained *K* and *m* parameters of a given set of amides, a Monte Carlo approach was taken where 150 samplings of a Gaussian distribution of width defined by estimates of the precision of the hydrogen exchange data (see above) was used.

Ideally, the first step in this analysis is to identify those amide hydrogens whose exchange is dominated by the contribution of global unfolding at high denaturant concentration and local unfolding at low denaturant concentrations and have no significant subglobal contribution. Identifying these amides amounts to finding those which show a linear dependence of ΔG_{HX}^{eff} upon GdmCl with the largest slope (*m*). Under these conditions, eq 6 is formally equivalent to the three parameter relationship defined by eq 4. A search for these amides led to the identification of 11 amides (residues 32−37, 70−71, and 75−77) which share a common *m* value of 5.4 kcal mol^{-1} M^{-1}, which is the largest found. The associated global free energy, ΔG_{HX}^{g}, is found to be 5.9 kcal mol^{-1}. It is important to note that this *m* value is very similar to the *m* value obtained by the LEM analysis (see above), indicating that the unfolding of this cooperative unit is associated with global unfolding. The grid search is summarized in Figure 7.

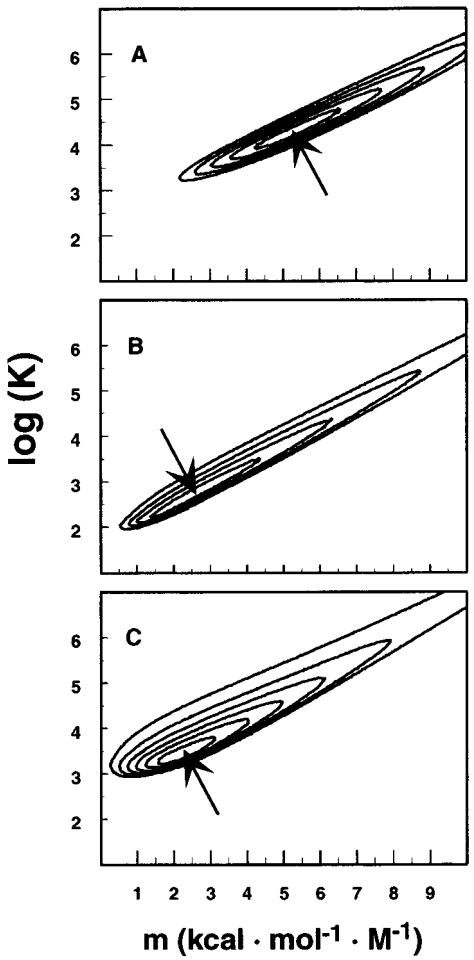

FIGURE 7: Identification of cooperative units of structure. Shown is a two-dimensional error grid defined by eq 7 calculated for the given set of amides defining the cooperative unit. Panel A shows the error grid defining the *K* and *m* parameters associated with the cooperative unit whose unfolding corresponds to global unfolding (cooperative unit I). Residues 32−37, 70−71, and 75−77 define the core of this unit (i.e., do not have significant local unfolding contributions to exchange, see text). Panels B and C show the error grids defining the *K* and *m* parameters associated with the cooperative units whose unfolding corresponds to a subglobal unfolding. Residues 87−91 define the core of cooperative unit II (panel B), and residues 14 through 17 define the core of cooperative unit III (panel C). The minimum of each grid corresponds to the ΔG_{HX} and *m* parameters which give the best fit to the hydrogen exchange data.

Given the global parameters, a similar search was carried out for additional sets of hydrogens which share a common subglobal parameter set. Again, a three-parameter fit formally equivalent to eq 4 is required where the global (now determined) and local (denaturant independent) terms are defined. Two additional sets were discovered having similar *m* values but distinct free energies. The core of one set involved four residues in helix I and had associated ΔG_{HX}^{sg} and m_{sg} parameters of 3.6 kcal mol^{-1} and 2.7 kcal mol^{-1} M^{-1}, respectively. The core of the other set involved five residues in helix IV and had associated ΔG_{HX}^{sg} and m_{sg} parameters of 4.8 kcal mol^{-1} and 2.6 kcal mol^{-1} M^{-1}, respectively. The grid searches are summarized in Figure 7 and the segregation in the ΔG_{HX}^{eff} versus GdmCl concentration plots shown in Figure 8. Even though they have very similar *m* values, helix I and helix IV appear to constitute separate cooperative units as they have distinct ΔG_{HX}^{sg}. This conclusion is further supported by the observation that combining them into a single group gives a sum of the squares of the residuals in the resulting fit greater than a factor of 2 than if they are fitted separately.

Given the core global and subglobal *K* and *m* parameters, each of the individual ΔG_{HX}^{eff} versus GdmCl data sets could then be fit for the local *K* and *m* parameters. Examples illustrating the goodness-of-fit are shown for helix II (Figure 8, panel D). The resulting global, subglobal and local *K* and *m* parameters are summarized in Table 1. Having defined the core *K* and *m* parameters, the obtained local parameters for residues whose exchange is largely local in nature is quite revealing. Plots of the local *m* parameters of residues adjoining the cores of each defined cooperative unit show a pattern indicative of the presence of helix end fraying. This is not unexpected; for small helices, the single sequence subset of the more general Zimm−Bragg (*40*) treatment of helix−coil transitions predicts a progressively smaller probability of hydrogen bond breakage as one moves from the ends of a helix to the interior (*41*). Accordingly, one would expect *m*, a rough measure of exposed surface area (*17*, *42*), to correlate in a similar manner as is shown in Figure 9. However, the relationship is not quantitative. This effect also results in a general reduction and leveling of the obtained local free energy parameters as the denaturant concentration increases. Interestingly, ΔG_{HX}^{loc} approaches a limit of ~2.7 kcal mol^{-1}, which is essentially the value seen for residues of helix I.

DISCUSSION

Equilibrium folding intermediates continue to provide insight into the principles underlying protein folding and stability. Apocytochrome b_{562} is an interesting example of a protein whose folding (and stability) is frustrated by the absence of a integral component of the final, native structure, a heme prosthetic group. Thus, in contrast to many models of metastable states of proteins generated by extreme conditions such as low pH, apocytochrome b_{562} may be studied under near native conditions which are directly applicable to the question of the folding and assembly of the protein into its final form. Apocytochrome b_{562} displays many of the characteristics of the classic protein molten globule such as a relatively low ΔC_p for unfolding, a relatively low cooperativity for unfolding, and a reduced stability relative to the holoprotein (*4*). Nevertheless, the protein is relatively structured and somewhat amenable to detailed structural characterization by NMR spectroscopy (*3*, *24*). The determination of the structure of apocytochrome b_{562} resolved issues surrounding the physical origin of many of the thermodynamic markers of the protein molten globule found for apocytochrome b_{562} (*3*). For example, rather than repack its interior to respond to the absence of the heme group, the protein retains its basic topology and largely maintains the heme cavity. The resulting exposure and solvation of a significant amount of hydrophobic surface area directly explains the origin of the low heat capacity changes seen upon unfolding. In addition, the mispacking at the interface between the first and second helices provides insight into the origin of the low stability and marginal cooperativity of the apoprotein.

The work presented here was undertaken to explore the range of local stabilities and cooperative structural units within apocytochrome b_{562}. Even under nondenaturing

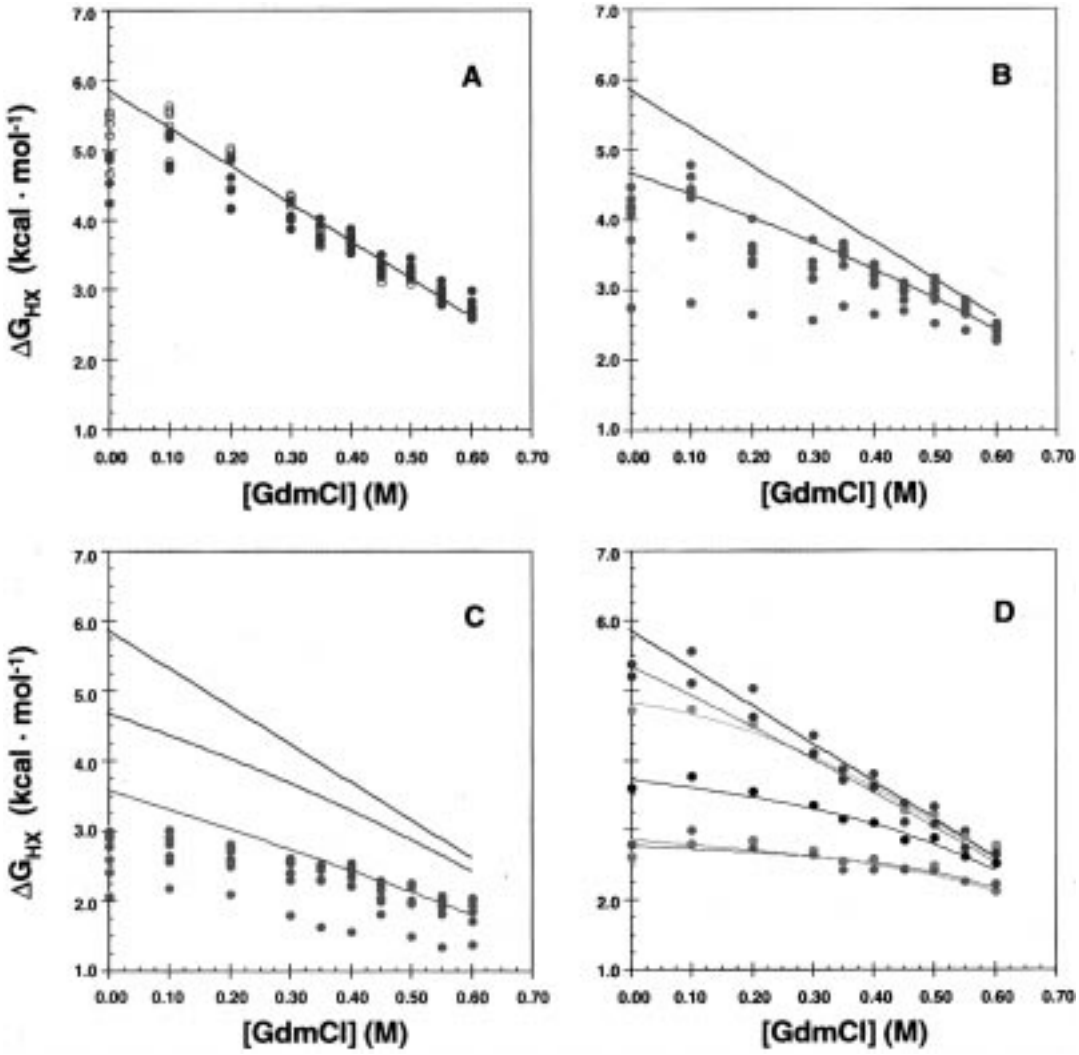

FIGURE 8: Segregation of individual amides into cooperative units on the basis of the dependence of ΔG_{HX}^{eff} on GdmCl concentration. Panel A corresponds to those data used to define the core of the cooperative unit I (see Figure 7). The blue line corresponds to eq 6 using the ΔG_{HX} and m values obtained for this cooperative unit. Panel B corresponds to those data used to define the core of the cooperative unit II (see Figure 7). The red line corresponds to eq 6 using the ΔG_{HX} and m values obtained for this cooperative unit and those of the more stable cooperative unit I. The corresponding line for cooperative unit I is also shown. Panel C corresponds to those data used to define the core of the cooperative unit III (see Figure 7). The green line corresponds to eq 6 using the ΔG_{HX} and m values obtained for this cooperative unit and the more stable cooperative unit I. The corresponding lines for cooperative units I and II are also shown. Panel D shows examples of fits to determine local parameters obtained for residues in helix II. Residues from ends and the central components of helix II are shown with the solid lines corresponding to the best fit of local parameters to the individual data sets. Note that in all cases, the ΔG_{HX} values shown are uncorrected for the proline effect (see text).

conditions, an ensemble of proteins is distributed over the full range of conformational states available to it with the population dictated by Boltzman weighting. Bai et al. (*14*, *37*) have illustrated how the binding of chemical denaturants can redistribute the protein ensemble over this set of states by varying their relative free energies. We have used this approach to dissect out the fundamental units of structure that compose the topology of the apoprotein and to provide insight into the folding pathway(s) available to it.

Global Stability. The partially folded structure of apocytochrome b_{562} has a heat capacity slightly lower than that of the unfolded state but nevertheless unfolds over a rather narrow range of temperature. This unfolding proceeds with excess heat absorption profile closely typical of a two-state transition. It should be mentioned that the ensemble of states detected here by hydrogen exchange methods have apparent thermodynamic parameters that would result in a multistate transition that would be effectively indistinguishable from a two-state transition. The fitted van't Hoff and direct calorimetric enthalpies are in reasonable agreement reinforcing the largely first-order phase transition character of the unfolding of this state of the protein. These results contrast sharply with those from α-lactalbumin and apomyoglobin under acidic conditions (*43*).

An interesting apparent paradox arises when comparing estimates of the free energy change for thermal unfolding measured by calorimetry ($\Delta G_{cal} \approx 5$ kcal mol^{-1}) with that obtained by linear extrapolation of GdmCl denaturation through the transition followed by CD ($\Delta G_{LEM} \approx 3.3$ kcal mol^{-1}) and with that obtained from analysis of hydrogen exchange ($\Delta G_{HX} \approx 5.9$ kcal mol^{-1}). The slow cis−trans isomerization of the prolyl peptide bond in the unfolded state(s) will lead to a discrepancy between ΔG_{Cal} and ΔG_{HX} as an equilibrium between the cis and trans forms will be reached in the calorimetric experiment but not in the hydrogen exchange experiment (*13*). Assuming that the cis:

Table 1: Obtained Subglobal and Local Hydrogen Exchange Parameters for Apocytochrome b_{562}[a]

residue	ΔG_{HX}^{sg} (kcal mol^{-1})	m_{sg} (kcal mol^{-1} M^{-1})	ΔG_{HX}^{loc} (kcal mol^{-1})	m_{local} (kcal mol^{-1} M^{-1})
E8			2.84(0.18)	0.00(0.00)
L10			2.25(0.13)	1.09(0.47)
N11			3.41(0.14)	0.00(0.00)
L14	3.61(0.40)	2.70(0.84)	3.56(0.15)	0.00(0.03)
K15	3.61(0.40)	2.70(0.84)	2.89(0.11)	0.00(0.01)
V16	3.61(0.40)	2.70(0.84)	3.50(0.16)	0.04(0.16)
I17	3.61(0.40)	2.70(0.84)	3.08(0.12)	0.60(0.53)
E18			2.81(0.11)	0.25(0.45)
K19			3.40(0.13)	0.00(0.02)
A20			3.59(0.16)	0.00(0.00)
Q25			2.80(0.06)	0.41(0.29)
V26			3.98(0.12)	2.47(0.45)
K27			5.20(0.17)	4.10(0.72)
D28			3.71(0.11)	1.04(0.47)
A29			5.68(0.27)	3.22(1.61)
L30			5.22(0.28)	4.77(0.74)
T31			5.19(0.22)	4.63(0.67)
K32	5.87(0.12)	5.39(0.27)	5.04(0.14)	2.06(1.05)
M33	5.87(0.12)	5.39(0.27)	6.43(0.56)	3.14(2.69)
R34	5.87(0.12)	5.39(0.27)	6.03(0.22)	0.56(1.63)
A35	5.87(0.12)	5.39(0.27)	6.36(0.17)	0.41(1.49)
A36	5.87(0.12)	5.39(0.27)	6.74(0.43)	2.48(2.75)
A37	5.87(0.12)	5.39(0.27)	6.32(0.26)	1.80(2.38)
L38			5.49(0.20)	5.02(0.68)
D39			4.93(0.14)	3.32(0.66)
A40			4.95(0.08)	0.45(0.78)
Q41			4.53(0.10)	1.55(0.74)
K42			3.74(0.09)	1.02(0.48)
A43			2.89(0.07)	0.68(0.24)
D66			2.83(0.11)	0.00(0.06)
I67			1.85(0.09)	0.81(0.23)
L68			4.12(0.12)	2.76(0.46)
V69			4.61(0.39)	3.45(0.85)
G70	5.87(0.12)	5.39(0.27)	4.72(0.15)	1.11(0.81)
Q71	5.87(0.12)	5.39(0.27)	5.21(0.33)	0.44(0.89)
I72			5.14(0.39)	4.38(0.88)
D73			4.66(0.22)	3.46(0.64)
A75	5.87(0.12)	5.39(0.27)	5.33(0.27)	0.00(0.00)
L76	5.87(0.12)	5.39(0.27)	5.32(0.50)	2.09(2.11)
K77	5.87(0.12)	5.39(0.27)	4.54(0.12)	0.15(0.38)
L78			4.87(0.31)	2.88(0.97)
A79			4.72(0.19)	2.96(0.69)
N80			4.76(0.19)	0.82(0.72)
A87	4.76(0.28)	2.62(0.81)	4.47(0.41)	1.25(2.11)
Q88	4.76(0.28)	2.62(0.81)	4.32(0.42)	1.70(1.56)
A89	4.76(0.28)	2.62(0.81)	5.78(1.02)	1.57(3.49)
A90	4.76(0.28)	2.62(0.81)	4.54(0.50)	1.36(2.25)
A91	4.76(0.28)	2.62(0.81)	4.81(0.57)	1.00(2.39)
E92			3.89(0.14)	0.46(0.53)
Q93			2.86(0.08)	0.03(0.10)

[a] Summary of hydrogen exchange parameters obtained at a nominal pH* of 4.5 and 25 °C. ΔG_{HX}^{g} and m_g are 5.87 ± 0.12 kcal mol^{-1} and 5.39 ± 0.27 kcal mol^{-1} M^{-1}, respectively. The values enclosed in parentheses are the standard error of the hydrogen exchange parameters obtained determined from a Monte Carlo sampling of the fitted ΔG_{HX}^{eff}. Subglobal parameters are provided only for those residues that were used to define them.

trans ratio is 1:4 in the unfolded states, ΔG_{HX} should be reduced by $RT\ln(1 + 0.25)$ for each of the four trans prolines in the folded state. This gives a corrected ΔG_{HX} of approximately 5.3 kcal mol^{-1} which is, considering the uncertainty in ΔC_p, in excellent agreement with the change in free energy obtained by calorimetry.

The apparent discrepancy between the calorimetric and hydrogen exchange estimates of the free energy for global unfolding and that obtained by the linear extrapolation method apparently resides in the nonlinear dependence of the latter on denaturant concentration (Figure 3). The

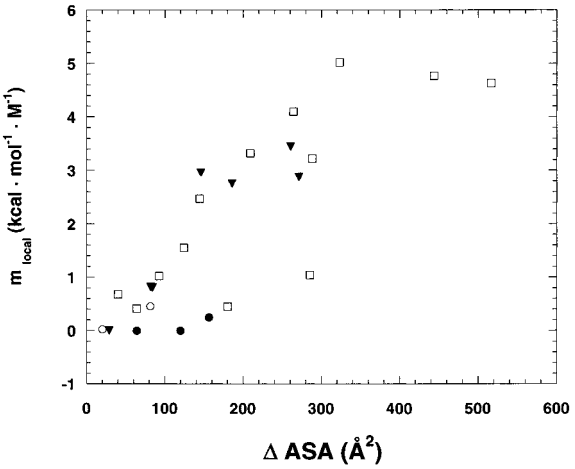

FIGURE 9: Relationship between local *m* values and changes in accessible surface area as predicted by helical end fraying from the folded state. Shown are the fitted local *m* values for those sites having significant local contributions to hydrogen exchange. Estimates of changes in accessible surface area were obtained assuming that the "open" residues are fully exposed to solvent. Shown is the cumulative accessible surface area assuming the single sequence limit of helical end fraying. Residues of helix I are indicated with closed circles (●), helix II with open squares (□), helix III with close triangles (▲) and helix IV with open circles (○).

denaturant binding model (*44*) provides for a nonlinear dependence of the free energy at low denaturant concentrations where

$$\Delta G = \Delta G(0) - \Delta nRT\ln(1 + K_b[\mathrm{Den}]) \qquad (8)$$

Application of this model to the data presented in Figure 3 results in an apparent Δn of 15.8 and an apparent equilibrium binding constant (K_b) of 0.69 M^{-1} having associated free energy change of 4.7 kcal mol^{-1}, which are consistent with values reported for proteins of similar size (*18*, *31*, *45*).

Subglobal Cooperative Units of Structural Stability. Three independent cooperatively stabilized units of structure have been identified by an objective analysis of the dependence of hydrogen exchange at 60 amide sites distributed across the sequence of apocytochrome b_{562}. The cooperative units have a narrow range of ΔG_{HX} of between 5.9 and 3.6 kcal mol^{-1}. The *m* values obtained range from 5.4 to 2.6 kcal mol^{-1} M^{-1}. Compared to other systems where this kind of study has been undertaken, this is a small dynamic range and required the quantitative analysis used. The most stable cooperative unit includes helices II and III, which are well packed in the structure of apocytochrome b_{562} and maintain an interhelical orientation that is similar to the holoprotein (*3*). The two least stable cooperative units of structure have nearly identical *m* values, which is consistent with the unfolding of the corresponding individual helices. Helix I consists of four turns that are poorly packed against the main body of the core of the molecule, helices II and III. Helix IV consists of three turns that are well packed against helices II and III. On the basis of the structure of apocytochrome b_{562} obtained under similar conditions, each is expected to have roughly the same change in accessible surface area upon unfolding (*3*). Accordingly, a similar *m* value is anticipated as is seen. It is important to note that the two helices do not appear to form a cooperative unit as they have distinct

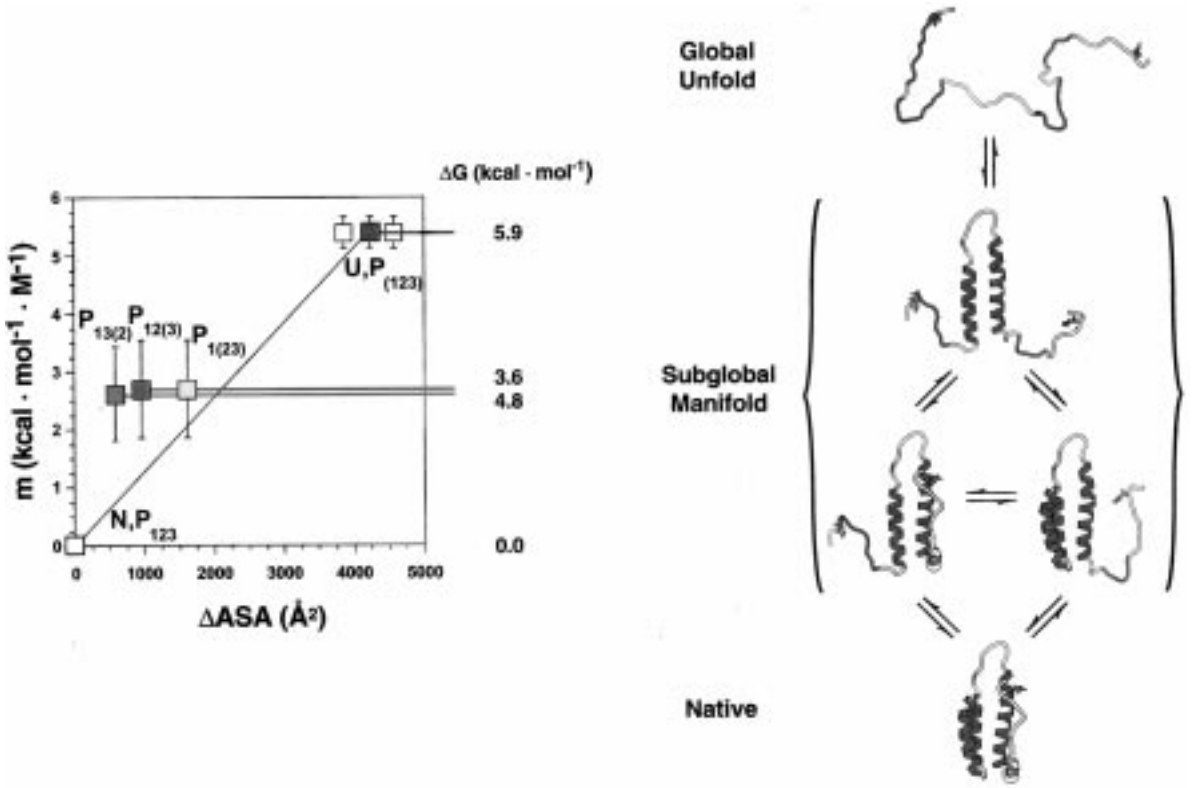

FIGURE 10: Insight into free energy ensemble of apocytochrome b_{562}. On the left is shown a plot of the obtained (sub)global *m* values for the three cooperative units of the protein versus the predicted change in accessible surface area. The uncertainty of *m* values are estimated from a Monte Carlo analysis. The uncertainty of accessible surface areas for the unfolded states were estimated by the procedure of Creamer et al. (*28*, *29*). The symbols are centered on the average accessible surface area changes. On the right is shown the minimal set of states indicated by the analysis presented here. See text for details.

ΔG_{HX}, which differ by 1 kcal mol^{-1}. Indeed, the structure indicates that there are no significant contacts between the first and fourth helices reinforcing the conclusion that the two helices form independent cooperative units of structure.

Local Dynamics of Cooperative Units of Structure. The analysis presented represents the first attempt to comprehensively determine local *K* and *m* parameters. The pattern of obtained ΔG_{HX}^{loc} and m_{loc} parameters indicates that helix end fraying is the dominant local motion giving rise to exchange competent states. It is not clear, however, that the obtained local *m* parameters simply correspond to the progressive addition of generic accessible surface area as the fraying includes increasingly longer portions of the helix (Figure 9). While the trend is qualitatively represented, *m* does not appear to simply scale with accessible surface area in a quantitative manner. Many factors may enter into the magnitude of *m* including the type of accessible surface area (i.e., charge, polarity, etc.) that is exposed (see ref *46* and references therein). Ultimately, one would hope that this kind of data would lead to a true calibration of *m* in terms of individual amino acid properties. Unfortunately, the data provided by apocytochrome b_{562} is of limited dynamic range and is of too limited precision to adequately address this issue. Other more suitable systems are currently being studied from this point of view.

An interesting feature is seen in the behavior of helix I which comprises the cooperative unit of lowest stability. The absence of significant end fraying detected by hydrogen exchange suggests two possible situations: that individual amides are able to open independently and do so with an effective free energy change that is common to all members or that the entire helix opens at once. The latter seems most likely and may reflect the cooperative instability of the helix, i.e., that the loss of even one hydrogen bond is sufficient to drive the total opening of the helix.

The Equilibrium Ensemble of Apocytochrome b_{562} and Potential Connections to the Folding Pathway. The structural states, distinguished by hydrogen-bonding, of apocytochrome b_{562} identified here represent those which dominate the ensemble of states present at equilibrium. A potentially very powerful capability of the use of the effects of chemical denaturants on hydrogen exchange behavior is the illumination of possible major intermediates of protein folding pathways (*14*, *37*). There are now several examples (*11*, *37*, *38*) where significant insight into the identity of major elements of a protein's folding pathway have been obtained by this approach. However, there are also examples where there is not a correspondence between structural states detected at equilibrium and kinetic intermediates (*36*, *47*). Indeed, these latter examples appear to be situations where subglobal opening(s) provide little or no contribution to the observed hydrogen exchange rates which are then effectively partitioned between local and global unfolding events as envisaged some time ago (*48*, *49*).

The appearance of a correspondence between structural states that are dominant at equilibrium and the structural states that are populated as intermediates during kinetic refolding requires a very specific extrathermodynamic restraint on the energy landscape describing the folding process, i.e., that the lowest free energy wells must be

associated with the highest barriers. While this is obviously not necessarily true, in the context of thermodynamically driven folding involving only native-like structure, it is likely to be largely operative. This remains to be seen. Nevertheless, despite the significant limitation that equilibrium measurements, such as those used here, cannot alone specify the precise order of a folding pathway, it is noted that considerable restrictions on possible pathways can in some cases be reliably deduced. For example, as noted by Bai et al. (*37*), a single compulsory sequential folding mechanism involving cooperative units or, in their terminology, partially unfolded forms, should show a linear relationship between the predicted change in accessible surface area upon their unfolding and the obtained subglobal *m* values. In the case of apocytochrome b_{562}, one sees from Figure 10 that the compulsory sequential addition of cooperative units II and III to a core formed by cooperative unit I can be ruled out. This is because they have effectively the same *m* value. Accordingly, a random and independent addition to the more stable core formed by cooperative unit I is suggested.

This particular result is not unlike the behavior seen for α-lactalbumin when examined by scanning proline mutagenesis (*50*) and progressive denaturation with chemical denaturant (*51*). In this particular molten globule, both of these studies indicate the absence of cooperative unfolding between units of secondary structure. Apocytochrome b_{562} displays a behavior more intermediate between a native protein structure and the molten globule state represented by α-lactalbumin. In apocytochrome b_{562}, the unfolding of the core involves cooperative interactions spanning the two central helices but the less stable peripheral helices show little cooperative interaction between each other or with respect to the core of the protein. This is in contrast to native state proteins where highly cooperative unfolding is generally observed and the essentially noncooperative disassembly seen in the α-lactalbumin molten globule (*50*, *51*).

Conclusions. The combined use of differential scanning calorimetry and the dependence of hydrogen exchange parameters on chemical denaturant has allowed the local, subglobal, and global stabilities of the structure of apocytochrome b_{562} to be dissected. A quantitative and objective method has been developed to identify cooperative units of structure. Three cooperative units of structure have been identified and the corresponding *m* and effective free energies suggest a random addition of helix I and IV to a core of helix II and III is a major element of the folding pathway for the protein. The analysis presented also reveals a semiquantitative relationship between local *m* values and helix fraying.

ACKNOWLEDGMENT

We gratefully acknowledge the technical assistance and advice of Ramona Bieber. We thank Professors Walter Englander, Peter Privalov, and Nick Pace for advice and comments on the manuscript and Dr. Clifford Robinson for sharing results prior to publication.

SUPPORTING INFORMATION AVAILABLE

One table listing ΔG_{HX}^{eff} values obtained at each GdmCl concentration used (2 pages). Ordering information is given on any current masthead page.

REFERENCES

1. Lederer, F., Glatigny, A., Bethge, P. H., Bellamy, H. D., and Matthew, F. S. (1981) *J. Mol. Biol. 148*, 427−48.
2. Hamada, K., Bethge, P. H., and Mathews, F. S. (1995) *J. Mol. Biol. 247*, 947−62.
3. Feng, Y., Sligar, S. G., and Wand, A. J. (1994) *Nat. Struct. Biol. 1*, 30−5.
4. Feng, Y., and Sligar, S. G. (1991) *Biochemistry 30*, 10150−5.
5. Hamada, D., Hoshino, M., Kataoka, M., Fink, A. L., and Goto, Y. (1993) *Biochemistry 32*, 10351−8.
6. Hughson, F. M., Wright, P. E., and Baldwin, R. L. (1990) *Science 249*, 1544−8.
7. Hughson, F. M., Barrick, D., and Baldwin, R. L. (1991) *Biochemistry 30*, 4113−8.
8. Cocco, M. J., and Lecomte, J. T. (1990) *Biochemistry 29*, 11067−72.
9. Eliezer, D., and Wright, P. E. (1996) *J. Mol. Biol. 263*, 531−8.
10. Falzone, C. J., Mayer, M. R., Whiteman, E. L., Moore, C. D., and Lecomte, J. T. J. (1996) *Biochemistry 35*, 6519−26.
11. Mayo, S. L., and Baldwin, R. L. (1993) *Science 262*, 873−6.
12. Kim, K. S., Fuchs, J. A., and Woodward, C. K. (1993) *Biochemistry 32*, 9600−8.
13. Bai, Y., Milne, J. S., Mayne, L., and Englander, S. W. (1994) *Proteins 20*, 4−14.
14. Bai, Y., and Englander, S. W. (1996) *Proteins 24*, 145−51.
15. Tanford, C. (1970) *Adv. Protein. Chem. 24*, 1−95.
16. Pace, C. N. (1975) *CRC Crit. Rev. Biochem. 3*, 1−43.
17. Schellman, J. A. (1978) *Biopolymers 17*, 1305−22.
18. Pace, C. N. (1986) *Methods Enzymol. 131*, 266−80.
19. Nikkila, H., Gennis, R. B., and Sligar, S. G. (1991) *Eur. J. Biochem. 202*, 309−13.
20. Robinson, C. R., and Sligar, S. G. (1993) *Protein Sci. 2*, 826−37.
21. Nozaki, Y. (1972) *Methods Enzymol. 26*, 43−50.
22. Kay, L. E., Keifer, P., and Saarinen, T. (1992) *J. Am. Chem. Soc. 114*, 10663−65.
23. Zhang, O., Kay, L. E., Olivier, J. P., and Forman-Kay, J. D. (1994) *J. Biomol. NMR 4*, 845−58.
24. Feng, Y., Wand, A. J., and Sligar, S. G. (1991) *Biochemistry 30*, 7711−7.
25. Press, W., Teukolsky, S., Vetterling, W., and Flannery, B. (1992) *Numerical Recipes in Fortran 77. The Art of Scientific Computing*, Cambridge University Press, Cambridge.
26. Bai, Y., Milne, J. S., Mayne, L., and Englander, S. W. (1993) *Proteins 17*, 75−86.
27. Connelly, G. P., Bai, Y., Jeng, M. F., and Englander, S. W. (1993) *Proteins 17*, 87−92.
28. Creamer, T. P., Srinivasan, R., and Rose, G. D. (1995) *Biochemistry 34*, 16245−50.
29. Creamer, T. P., Srinivasan, R., and Rose, G. D. (1997) *Biochemistry 36*, 2832−5.
30. Pfeil, W., and Privalov, P. L. (1976) *Biophys. Chem. 4*, 33−40.
31. Makhatadze, G. I., and Privalov, P. L. (1992) *J. Mol. Biol. 226*, 491−505.
32. Johnson, C. M., and Fersht, A. R. (1995) *Biochemistry 34*, 6795−804.
33. Hvidt, A., and Nielsen, S. O. (1966) *Adv. Protein. Chem. 21*, 287−386.
34. Englander, S. W., and Kallenbach, N. R. (1984) *Q. Rev. Biophys. 16*, 521−655.
35. Laidig, K. E., and Daggett, V. (1996) *Folding Des. 1*, 335−46.
36. Clarke, J., and Fersht, A. R. (1996) *Folding Des. 1*, 243−54.
37. Bai, Y., Sosnick, T. R., Mayne, L., and Englander, S. W. (1995) *Science 269*, 192−7.
38. Chamberlain, A. K., Handel, T. M., and Marqusee, S. (1996) *Nat. Struct. Biol. 3*, 782−7.
39. Dellwo, M. J., and Wand, A. J. (1989) *J. Am. Chem. Soc. 111*, 4571−8.
40. Zimm, B. H., and Bragg, J. K. (1959) *J. Chem. Phys. 31*, 526−35.

41. Qian, H., and Schellman, J. A. (1992) *J. Phys. Chem. 96*, 3987−94.
42. Myers, J. K., Pace, C. N., and Scholtz, J. M. (1995) *Protein Sci. 4*, 2138−48.
43. Griko, Y. V., and Privalov, P. L. (1994) *J. Mol. Biol. 235*, 1318−25.
44. Aune, K. C., and Tanford, C. (1969) *Biochemistry 8*, 4586−90.
45. Pace, C. N., and Vanderburg, K. E. (1979) *Biochemistry 18*, 288−92.
46. DeKoster, G. T., and Robertson, A. D. (1997) *Biophys. Chem. 64*, 59−68.
47. Itzhaki, L. S., Neira, J. L., and Fersht, A. R. (1997) *J. Mol. Biol. 270*, 89−98.
48. Privalov, P. L., and Tsalkova, T. N. (1979) *Nature 280*, 693−6.
49. Woodward, C. K., and Hilton, B. D. (1980) *Biophys. J. 32*, 561−75.
50. Schulman, B. A., and Kim, P. S. (1996) *Nat. Struc. Biol. 3*, 682−87.
51. Schulman, B. A., Kim, P. S., Dobson, C. M., and Redfield, C. (1997) *Nat. Struct. Biol. 4*, 630−34.
52. Kraulis, P. J. (1991) *J. Appl. Crystallogr. 24*, 946−950.
53. Nicholls, A., Sharp, K. A., and Honig, B. (1991) *Proteins 11*, 281−96.

BI972579S